Enhancement of the in-plane effective mass of electrons in modulation-doped $In_xGa_{1-x}As$ quantum wells due to confinement effects

G. Hendorfer
Institut für Experimentalphysik, Universität Linz, Altenberger Straße 69, A-4040 Linz, Austria

M. Seto
Institut für Halbleiterphysik, Universität Linz, Altenberger Straße 69, A-4040 Linz, Austria

H. Ruckser and W. Jantsch
Institut für Experimentalphysik, Universität Linz, Altenberger Straße 69, A-4040 Linz, Austria

M. Helm and G. Brunthaler
Institut für Halbleiterphysik, Universität Linz, Altenberger Straße 69, A-4040 Linz, Austria

W. Jost, H. Obloh, and K. Köhler
Fraunhofer Institut für Angewandte Festkörperphysik, Tullastraße 72, D-7800 Freiburg, Germany

D. J. As
Heinrich-Hertz-Institut für Nachrichtentechnik, Einsteinufer 37, D-1000 Berlin, Germany
(Received 28 December 1992; revised manuscript received 18 March 1993)

We present investigations on the in-plane effective mass of conduction electrons in pseudomorphic, strained $GaAs/In_xGa_{1-x}As/Al_yGa_{1-y}As$ quantum wells. The samples are modulation doped by silicon leading to electron sheet densities in the range of 10^{12} cm^{-2} in the $In_xGa_{1-x}As$ layers. In photoluminescence experiments at low temperature we observe that all electrons of the two-dimensional electron gas up to the Fermi energy contribute to the luminescence. This leads to an asymmetric broadening of the luminescence line shape and indicates a breakdown of the **k**-conservation rule. This offers the possibility of determining the Fermi energy from the low-temperature spectra. From contactless microwave Shubnikov–de Haas measurements we determine a quantity correlated to the sheet carrier density. By combining both methods we deduce the in-plane effective electronic mass and investigate its dependence on confinement. We observe a slight increase of the mass due to the built-in strain of the pseudomorphic layers and a strong increase due to confinement effects by up to 40% for 2-nm wells. Self-consistent calculations of the electronic-energy levels, the wave functions, and the perpendicular effective mass show that the observed dependence of the effective mass on the confinement is supported from a theoretical point of view. We compare the in-plane effective mass with the perpendicular one.

I. INTRODUCTION

Pseudomorphic, strained $Al_xGa_{1-x}As/In_xGa_{1-x}As/GaAs$ high electron mobility transistor structures (HEMT) are of great interest for high speed device applications. In this material, both the alloy composition and the built-in strain offer additional degrees of freedom for band-structure tailoring.[1] In addition, better confinement of the two-dimensional (2D) electrons[2] as well as a lower effective mass is achieved than in $GaAs/Al_xGa_{1-x}As$ HEMT structures.

The effective mass of the 2D conduction electrons, however, is expected to be strongly modified by confinement,[3,4] as well as by strain.[5–7] The mass also is split into two components according to motion parallel and perpendicular to the layers, respectively. The parallel mass determines the electron mobility and is therefore of great technological importance. The perpendicular mass determines the quantization energy of electrons and therefore governs the spectral position of absorption or luminescence lines.

The strain-induced anisotropy is predicted to increase monotonically with increasing In model fraction x.[5] It is expected to be smaller than 5%, even for the sample with the highest x value ($x=0.35$) used in our investigation. There should be, however, also a strain-induced isotropic shift of the effective mass of the order of 20% for the above sample.

The confinement-induced enhancement of the effective mass has been treated theoretically by Ekenberg for $GaAs/Al_xGa_{1-x}As$ quantum wells (QW's). He attributed this effect to the nonparabolicity of the conduction band on the confinement energy and to the penetration of the wave function into the barriers.[4] He predicted that the enhancement effect on the parallel mass is about three times larger than the one on the perpendicular mass for $GaAs/Al_xGa_{1-x}As$ QW's.

Most recently, a systematic investigation of the depen-

dence of the in-plane effective mass of electrons in $In_xGa_{1-x}As/InP$ QW's on the QW width has been published by Wetzel *et al.*[8] As experimental method, they used optically detected cyclotron resonance.[9] Since they investigated lattice-matched material, strain effects were unimportant. They observed an effective-mass enhancement with decreasing well width down to 8 nm. For smaller QW widths the signal-to-noise ratio of their method was not sufficient to allow determination of the effective mass with the exception of one sample with a 5-nm QW width. From this sample, however, a much smaller mass enhancement is obtained than in the case of the 8-nm sample. This is surprising because it is in disagreement with Ekenberg's work, which predicts a monotonic characteristic.

In this paper we show that the in-plane effective mass of modulation-doped $GaAs/In_xGa_{1-x}As/Al_xGa_{1-x}As$ QW's increases strongly and monotonically with decreasing QW width. We also observe a slight increase of the mass with the strain of the QW's. The in-plane mass is determined by evaluating both photolunminescence and Shubnikov–de Haas experiments. In addition, we calculate the perpendicular effective mass self-consistently. By comparing the experimental results with the self-consistent calculation we obtain a ratio of the confinement-induced enhancement factors for the masses parallel and perpendicular to the layers which is smaller than Ekenberg's prediction given in Ref. 4.

II. SAMPLES

The heterostructures investigated were grown by molecular-beam epitaxy and contain a high-electron mobility transistor (HEMT) structure grown on semi-insulating LEC(100) GaAs. They consist of a 300-nm undoped GaAs buffer layer, a $GaAs/Al_xGa_{1-x}As$ superlattice, and a 600-nm undoped GaAs layer, followed by the $In_xGa_{1-x}As$ QW (see inset in Fig. 2). Samples were studied with well widths and InAs mole fractions ranging from 2 to 16 nm and from 0.2 to 0.39, respectively. On top of that active region a 5-nm undoped $Al_{0.3}Ga_{0.7}As$ spacer layer is grown, followed by a 1.7-nm-wide GaAs QW with a Si- δ doping of 3.5×10^{12} cm^{-2} and a 60-nm-wide $Al_{0.3}Ga_{0.7}As$ layer. The structure is capped by a 20-nm GaAs layer. The low-temperature mobility of the samples investigated is of the order of 10^5.

III. EXPERIMENT

For the photolunminescence experiments a BOMEM-DA 8.22 Fourier spectrometer was employed. The samples were cooled to 5 K by using a continuous-flow cryostat. The luminescence was excited with an argon-ion laser emitting at 514 nm at an excitation intensity of typically 0.1–1 W/cm^2.

The Shubnikov–de Haas (SdH) measurements were performed with a BRUKER electron paramagnetic resonance (EPR) spectrometer which allows us to record the microwave absorption as a function of the magnetic field. The microwave absorption is detected via the cavity quality factor which changes due to the variation of the longitudinal resistance with magnetic field. This method enables a quick and very accurate determination of the electron concentration and an estimation of the mobility without the necessity to put contacts on the samples.[10,11] In addition, if samples with more than one electronic subsystem are investigated, they can be analyzed independently of each other as described in the following section. The sample temperature in these kind of experiments was 5 K as well.

IV. RESULTS AND DISCUSSION

The SdH effect yields oscillations of the longitudinal resistivity that are periodic with respect to the inverse magnetic field. From the period $\Delta(1/B)$, according to Eq. (1), the product $(E_F-E_1)\times m_{II}$ can be determined, where E_1 and E_F are the energy of the first electronic subband and the Fermi energy, respectively, and m_{II} is the parallel effective mass,

$$\Delta\left[\frac{1}{B}\right]=\frac{he}{2\pi(E_F-E_1)m_{II}} . \tag{1}$$

If two-dimensional systems are investigated, m_{II} represents the in-plane effective mass of electrons at the Fermi energy.[12] It is helpful to count E_F and E_1 from the maximum of the first heavy-hole subband, because these quantities can then be taken directly from the photoluminescence spectra (see below). The sheet density n_{2D} can be evaluated from the period according to Eq. (2) which is strictly valid only for parabolic bands,

$$n_{2D}=\left[\frac{2e}{h}\right]\frac{1}{\Delta\left[\frac{1}{B}\right]} . \tag{2}$$

In Fig. 1, the SdH effect of a quantum-well structure with a well width of 6 nm is shown. A Fourier analysis of this signal is shown in Fig. 2. In the samples investigated only one subband is filled at low temperatures. Hence, the corresponding SdH spectra exhibit only one oscillation frequency. The peak position indicates the electron

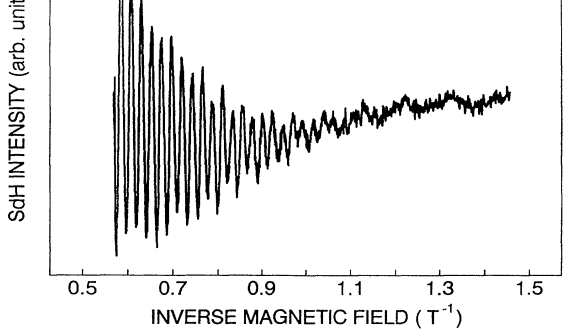

FIG. 1. Shubnikov–de Haas amplitude vs the inverse magnetic field.

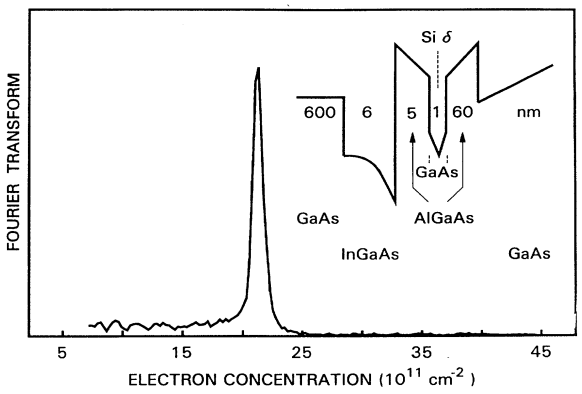

FIG. 2. Fourier transform of the signal in Fig. 1. In the inset the structure is shown.

sheet density which is defined according to Eq. (2). In the inset the structure of this representative sample is shown. We investigated the SdH oscillations also under illumination of laser radiation. The period of the SdH oscillations and, hence, the electron density did not change with this illumination.

The photoluminescence experiments of the HEMT structures reveal a typical line shape.[12] The origin of this photoluminescence line is a transition from the first electronic subband to the first subband of the heavy holes ($e1h1$ transition). Light-hole correlated transitions cannot be observed, since the light-hole states are shifted towards higher energy due to confinement and strain and are, therefore, not occupied at low temperature. Figure 3 shows two spectra originating from two identical samples differing only in the QW widths. The shape of the luminescence lines is strongly asymmetric. It can be well described by a Gaussian shape on the low-energy side and a modified Lorentzian shape on the high-energy side of the peak (see below). The line exhibits a peak at a photon energy E_1, which is given by the sum of the renormalized

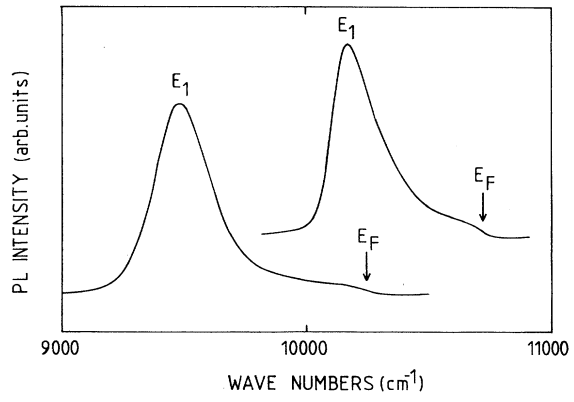

FIG. 3. Typical photoluminescence line shape of the single quantum-well structures investigated. The steplike structures on the high-energy side of the spectra indicated by arrows mark the Fermi energy.

energy gap and the electron and hole quantization energy, respectively. On the tail of the high-energy side of the peak, the luminescence intensity exhibits a rounded steplike structure indicated by arrows in Fig. 3.

The luminescence is attributed to electron-hole recombination within the $In_xGa_{1-x}As$ QW. Because of their rapid energy relaxation the photogenerated holes are located in k space close to the valence-band maximum of the first quantized heavy-hole state. The majority of the electrons are already present before excitation and are spread energetically between the first quantized electronic state and the quasi-Fermi energy. The quasi-Fermi energy is close to the Fermi level which, strictly speaking, is defined only in thermal equilibrium.

If the conservation of the $\mathbf{k}$ vector held strictly, only electrons with $\mathbf{k}\approx 0$ would contribute to the luminescence. The linewidth of the luminescence would then be expected to be very small and the line shape should be symmetric and Gaussian.

The fact that the linewidth is broadened so strongly on the high-energy side also indicates that electrons above the minimum of the first subband recombine with the photogenerated holes, thus breaking the $\mathbf{k}$-conservation rule. Such forbidden transitions are usually encountered in degenerate QW's,[13,14] and they can be attributed to (i) a breaking of the in-plane translation symmetry due to a localization of minority carriers,[15,16] or (ii) ionized impurity scattering which introduces higher-order impurity-assisted processes.[17] Minority carrier localization (i) may result from lateral fluctuations of the QW width, the In composition,[18] and the Coulomb potential.[19] In addition, there exists another line broadening mechanism in degenerate QW's which is explained by many-body effects. This is the so-called Fermi-edge singularity or Fermi enhancement,[15,20] resulting in a very strong peak at the quasi-Fermi energy. In none of our samples, however, do we observe a Fermi enhancement in photoluminescence experiments. Therefore, the most probable origin for the line broadening observed in our investigation is a relaxation of the $\mathbf{k}$ conservation rule due to hole localization, as described, for example in Ref. 20.

The Gaussian shape on the low-energy (left-hand) side of the photoluminescence (PL) maximum can be attributed to the usual inhomogeneous broadening mechanisms such as interface roughness or alloy inhomogeneity.[21] The same mechanisms, of course, also broaden the right-hand side of the spectra. This side, however, is broadened due to the indirect transitions. The line shape of this side is Lorentzian. The sharp decrease of the PL intensity on the high-energy tail reflects the Fermi-Dirac distribution of electrons at low temperature. We have simulated our spectra by convoluting the overall line shape with a Fermi-Dirac distribution function. This procedure yields the Fermi energy. The left-hand Gaussian side halfwidth of our spectra varies between 3 and 16 meV and the right-hand Lorentzian side halfwidth is proportional to the former; it is, however, increased by 30% to 100%.

In our samples, E_F-E_1 is typically 50 meV which makes nonparabolic corrections necessary. Therefore, Eq. (2) is valid approximately only. Nevertheless,

$(E_F-E_1)^*m_{II}$ can be determined with help of Eq. (1) from SdH measurements. Equation (1) is strictly correct, if m_{II} is taken as the nonparabolic energy-dependent in-plane effective mass. Dividing this quantity by (E_F-E_1), which is taken from PL measurements, yields the in-plane effective mass of electrons at the Fermi energy. We observe a strong increase of $m_{II}(E_F)$ with decreasing QW width which exceeds the corresponding bulk mass by about 40% at 2 nm.

For a quantitative description of this confinement effect on m_{II} we introduce the mass enhancement relative to its bulk value. This quantity allows us to also compare samples with different In concentrations. For the latter both alloy and strain effects have to be taken into account. Alloying causes a decrease of the effective mass with increasing In concentration.[22] This effect, however, is attenuated by strain which, according to theoretical predictions, causes an increase of the effective mass.[5-7] These expectations have been supported also by cyclotron resonance experiments[23] on $In_xGa_{1-x}As/GaAs$ QW's, where an electronic subband mass of approximately 0.075 was measured for In mole fractions up to 0.2. Brugger *et al.*[12] have measured an effective mass of 0.071 for $GaAs/In_xGa_{1-x}As/Al_xGa_{1-x}As$ QW's. They published, however, only this single experimental value although they investigated samples with different In mole fractions and different quantum-well widths. The effective-mass enhancement factors in Refs. 23 and 12 are 1.23 and 1.16, respectively.

In Fig. 4, the effective-mass enhancement factors are plotted as a function of the QW width. For QW widths of 9 and 13 nm, respectively, the enhancement factors are close to unity, reflecting a bulklike situation. In both cases, the present measurements yield a mass of 0.063 corresponding to the enhancement factor of 1.[5] These points have been obtained for $In_{0.2}Ga_{0.8}As$. The effective mass attributed to strain-free $In_{0.2}Ga_{0.8}As$ is 0.055.[22] This demonstrates that the effect of strain on the effective mass is evident even at relatively low In concentrations, and has to be taken into account if pseudomorphic layers are designed for fast devices. For QW widths smaller than 7 nm the effective mass starts to increase. Nonparabolicity and the admixture of the barrier mass due to barrier penetration of the wave function are the mechanisms responsible for this effect, as will be shown in the next section. The measured mass enhancement factor within the experimental error of approximately 15% increases monotonically with decreasing well width. The largest enhancement factor measured for a QW width of 2 nm equals, approximately, 1.4. Ekenberg has calculated the confinement effects due to the above mechanisms for $GaAs/Al_xGa_{1-x}As$ QW's.[4] He also predicted that the ratio of the enhancement of the effective masses parallel and normal to the layer is 3.2. We have calculated the energy and the wave function of electrons for our structure self-consistently, as shown in the next section. From these results we calculated the perpendicular mass and, subsequently, by assuming Ekenberg's relation[4] between the two mass components also the in-plane mass for comparison with our experimental results. In contrast to Ekenberg's theoretical work on $GaAs/Al_xGa_{1-x}As$ QW's we deduce a ratio of 1.7 for the confinement effect of the two mass components in $GaAs/In_xGa_{1-x}As/Al_xGa_{1-x}As$ QW's.

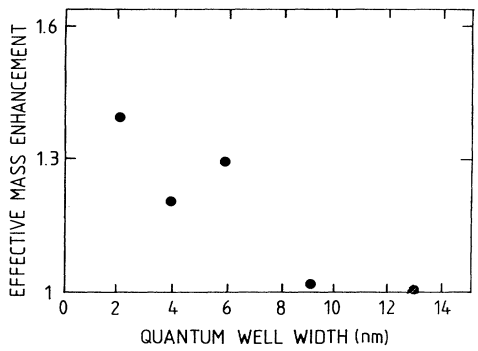

FIG. 4. Experimentally obtained enhancement of the in-plane effective masses vs quantum-well widths. A monotonic confinement induced increase of the masses is observed.

V. SELF-CONSISTENT CALCULATIONS

The energy level and the eigenfunction of the quantum-well ground state is calculated self-consistently by solving Schrödinger's and Poisson's equations simultaneously. For this procedure we take surface effects explicitly into account. By applying a two-band $\mathbf{k}\cdot\mathbf{p}$ model we derive an energy- and position-dependent effective mass for the conduction electrons. This mass is then averaged over the HEMT structure, weighted with the probability density to yield a phenomenological perpendicular effective mass for electrons in the $In_xGa_{1-x}As$ wells.

For semiconductor heterostructures, Schrödinger's and Poisson's equations can be written as one-dimensional, second-order differential equations,

$$\frac{d^2\psi}{dz^2}+k^2\psi=0\ , \tag{3}$$

$$\frac{d^2\phi}{dz^2}=\frac{-N(z)}{\varepsilon}\ , \tag{4}$$

where

$$k=\left[\frac{2m^*}{\hbar^2}(E-V)\right]^{1/2}\ , \tag{5}$$

and

$$V=V_h-e\phi+V_{\text{other}}\ . \tag{6}$$

Here, ψ is the eigenfunction, E the eigenenergy, V the total potential, z the position along the crystal-growth direction, and m^* the effective mass. ϕ is the electric potential, ε the material dielectric constant, and $N(z)$ the three-dimensional spatial concentration. V consists of the following three parts: V_h is the bare heterostructure confining potential, arising from band-gap discontinuities, $-e\phi$ is the electrostatic energy, and V_{other}, in our case, consists only of the exchange-correlation energy

correction.

We solved Schrödinger's equation using Kane's transfer-matrix method, whereby the potential V is broken up into small piecewise constant potential steps.[24,25] The potential in Schrödinger's equation is $V_h - e\phi + V_{\text{other}}$. As has already been defined, V_h is the bare heterostructure potential and can serve as the first trial potential within Eq. (1). ϕ is obtained from the solution to Poisson's equation in one dimension, which can be taken simply as

$$\phi(z)=\frac{e}{\varepsilon}\int_{-\infty}^{z} dz'(z-z')N(z') \tag{7}$$

with

$$N(z)=N_D(z)-\sum_j n_j|\psi_j|^2 , \tag{8}$$

where N_D is the 3D donor doping profile and n_j is the areal electron concentration in the jth subband.

The V_{other} considered by us consists of exchange-correlation energy correction due to many-body interactions of an electron gas. We employ the parametrized formulation of the exchange-correlation energy according to Ref. 26.

The occupation of each subband, found in Eq. (8), is determined by the Fermi-Dirac distribution function. The 2D concentration on the jth subband is[27]

$$n_j=\frac{\langle 1/m^* \rangle^{-1}}{\pi\hbar^2} kT \ln\left[1+\exp\left[\frac{E_F-E_j}{kT}\right]\right] , \tag{9}$$

where k is Boltzmann's constant. Naturally, n_j should also be properly normalized by

$$n_s=N_D d=\sum_j n_j \tag{10}$$

to ensure change conservation. n_s is the total areal electron concentration, and d is the thickness of the doping layer. Note that $\langle 1/m^* \rangle^{-1}$ is used for the "average" effective mass over a subband level.[3] (We will discuss this more carefully below.)

References to the mass so far refer exclusively to the perpendicular effective mass. Within the two-band $\mathbf{k}\cdot\mathbf{p}$ model it is given by

$$m_\perp^* = m_0^*\left[1+\alpha\frac{E-V}{E_g}\right] , \tag{11}$$

where m_0^* is the electron effective mass of the bulk material, and E_g is the material band gap. α is a factor equal to 2. In more complex models considering more than two bands, it has been shown that the effective mass can still be expressed in the form of Eq. (11), however with a factor α slightly less than 2.[4,28]

Calculations have also been done to determine the effect of quantum confinement upon the in-plane effective mass.[4] The relation is given as

$$\begin{aligned} m_\parallel^* &= m_0^*\left[1-(2\alpha+\beta)\frac{E-V}{E_g}\right]^{-1} \\ &\cong m_0^*\left[1+(2\alpha+\beta)\frac{E-V}{E_g}\right] , \end{aligned} \tag{12}$$

where β is another material constant related to conduction band and mass anisotropies. As α and β are nonparabolic corrections, they are small for $In_xGa_{1-x}As$, and so the approximation in (12) should hold. Taking the ratio of the difference of the in-plane mass to the difference of the perpendicular mass from the bulk material mass, one arrives at a very simple constant relation, as the energy dependence conveniently cancels

$$\frac{m_\parallel^*-m_0^*}{m_\perp^*-m_0^*}=\frac{2\alpha+\beta}{\alpha} . \tag{13}$$

Expression (13) is approximately equal to 3.2 for GaAs quantum wells.[4]

With a wave function that has a certain probability over a varying potential structure $V(z)$, it is not so clear cut as to what the effective mass is over a subband. In other words, m^* is also a function of z. Therefore, m^* has to be averaged over the entire subband.[3] The "average" effective mass can be calculated by[3]

$$\left\langle\frac{1}{m^*}\right\rangle=\int_{-\infty}^{\infty} dz\,\psi^*\frac{1}{m^*(z)}\psi . \tag{14}$$

This is the effective mass that is used in (11) and is what is used as a comparison with the experimental results.

The real quantum-well samples were sufficiently close to the surface that they afforded a serendipitous opportunity to verify its influence. So, incorporated into our calculations is that of surface states acquiring a number of electrons originating from the dopant. It is well established,[29,30] that there exist a large charge reservoir associated with dangling bonds at the surface, such that the Fermi energy is effectively pinned approximately mid band gap, at the surface. This has been experimentally determined by most to be about 650 meV below the conduction band. We included this Fermi-level pinning in our model. A good starting approximation for the amount of charge taken out of the wells and put onto the surface can be found by considering the surface and the doping-QW layers as simply two capacitor plates. Using this simplified model, the energy-charge relation is

$$U=\frac{e^2}{\varepsilon}n^{\text{surf}}d , \tag{15}$$

where n^{surf} is the resulting 2D charge density at the surface and d is the distance from the doping-QW region to the surface. These surface charges n^{surf} enter into Poisson's equation (7), and the charge conservation relation (10), i.e., $N_D d=n_s+n^{\text{surf}}$. Charges acquired by the surface must be compensated by a loss of charges n_s within the wells.

A typical result of the self-consistent calculation is shown in Fig. 5 where the first ground state, the corresponding wave function, and the Fermi energy level are

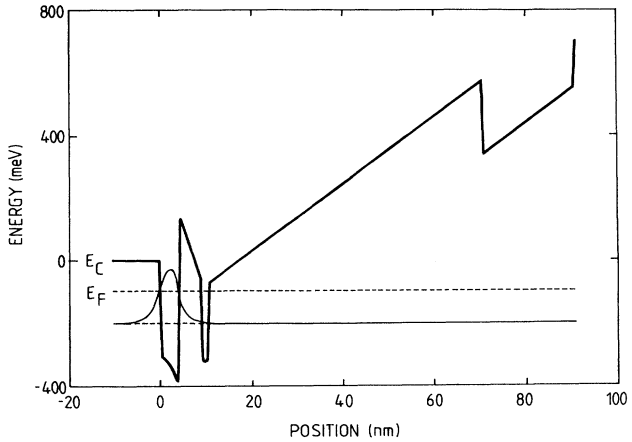

FIG. 5. Conduction-band potential at equilibrium. Only the first eigenvalue and the first eigenfunction is shown. E_F denotes the Fermi energy.

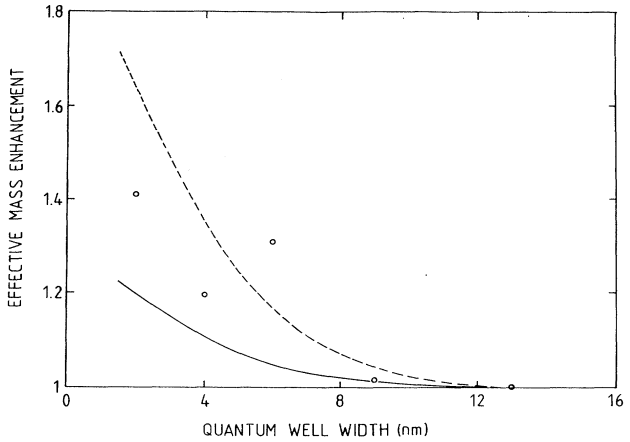

FIG. 6. Calculated and measured effective mass plotted vs the quantum-well width. The solid line represents the theoretical perpendicular mass. Above that curve the experimentally determined in-plane masses are shown as crosses. The dashed curve is obtained from the solid one by multiplying the confinement-induced increase of the perpendicular mass by a factor of 3.2. This ratio has been suggested for GaAs. In our case, a ratio of 1.7 is obtained for $In_xGa_{1-x}As$.

given. Note the extreme band bending of the $In_xGa_{1-x}As$ well on the side next to the δ-doped layer. This is due to an extremely large electric field between the positively charged doped region and the electrons in the well.

Using Eq. (15), one arrives at about $n=7.4\times10^{11}$ cm^{-2} moved to the surface. This agrees well with the final self-consistent result. This means approximately 57% of all the charges originally used for doping are bound by the surface states. This large percentage naturally affects the final results significantly. Note also the large electric field near the surface resulting from the charge transfer. The calculated concentration of the sheet density of the first subband agrees well with that measured by Subnikov–de Haas. This is a very good indication that the surface states were properly considered, as the concentration would naturally be very different should there have been no charge transfer.

As predicted, the calculated average effective mass of electrons occupying the first subband does increase with smaller well width. This can be easily explained by the fact that with smaller well width, the energy level gets pushed upwards towards the continuum. So as $E-V$ [Eq. (12)] increases, the nonparabolic term of the effective mass increases. As expected, the measured masses which are in-plane masses are larger than that of the perpendicular mass, shown in Fig. 6. The solid curve is for the calculated perpendicular mass for different well widths. The dashed curve represents the in-plane mass, using simply Eq. (13) and the GaAs parameters for the quantities α and β. While the perpendicular masses are the results of the self-consistent procedure, the in-plane mass is inferred from the former using Ekenberg's relation in Eq. (13). A ratio of 1.7 for the confinement-induced increase of the masses parallel and perpendicular to the layers needs to be used to obtain better agreement between the measured and the calculated in-plane masses. This value is nearly half of that suggested by Ekenberg in Ref. 4 for GaAs QW's.

The photoluminescence data are shifted by 10 meV relative to what is theoretically calculated. Because of the complexity of doing similar calculations for holes, we approximated the hole state as being at the very uppermost part of the valence band (recall that the valence band will be bent in a similar fashion as that shown in Fig. 5.) This would be a good approximation if the effective hole mass is very large. The energy difference between the first eigenenergy and this part of the valence band was used to estimate the PL data. The calculated energies are consistently lower than those measured, most probably because the hole state is, in fact, not exactly at the very valence-band edge. Nonetheless, the drastic increase in absorption energy is reflected theoretically for very small well widths.

VI. SUMMARY

In summary, we have investigated pseudomorphic strained modulation-doped $In_xGa_{1-x}As$ QW's by means of PL and SdH experiments. By modeling the PL line shape and by combining the results of both methods we determined the in-plane effective mass of conduction electrons within the QW's. We have observed a strong increase of these masses with decreasing QW width. We also calculated the electron energy levels and wave functions of our structures self-consistently. From these results we calculated the perpendicular masses, too.

We found that both mass components under confinement conditions follow the same tendency. However, the confinement-induced increase of the mass is by a factor of 1.7 larger for in-plane masses than for perpendicular masses. This experimentally obtained factor of 1.7 for $In_xGa_{1-x}As$ is about half of the value Ekenberg expected for GaAs.

ACKNOWLEDGMENTS

We would like to thank U. Kaufmann for his interest and his contribution to this work. We also thank A. U. Nurmikko for discussions. We are especially grateful to P. Ganser, who grew the samples. The work is supported from the Fonds zur Förderung der wissenschaftlichen Forschung.

[1]D. J. Dunstan and A. R. Adams, Semicond. Sci. Technol. **5**, 1202 (1990).

[2]A. A. Ketterson, W. T. Masselnik, J. S. Gedymin, J. Klem, C. K. Peng., W. F. Kopp, H. Morkoc, and K. R. Gleason, IEEE Trans. Electron Devices **ED-33**, 564 (1986).

[3]G. Bastard, *Wave Mechanics Applied to Semiconductor Heterostructures* (Les Editions de Physique, Les Ulis, 1988).

[4]U. Ekenberg, Phys. Rev. B **36**, 6152 (1987).

[5]G. Hendorfer and J. Schneider, Semicond. Sci. Technol. **6**, 595 (1991).

[6]R. People and S. Sputz, Phys. Rev. B **41**, 8431 (1990).

[7]M. Jaffe and J. Singh, J. Appl. Phys. **65**, 329 (1989).

[8]C. Wetzel, AI. L. Efros, A. Moll, B. K. Meyer, P. Omling, and P. Sobkowicz, Phys. Rev. B **45**, 14 052 (1992).

[9]C. Cavenett and E. J. Pakulis, Phys. Rev. B **32**, 8449 (1985).

[10]W. Jantsch, Phys. Scr. **T25**, 336 (1989).

[11]W. Timelthaler, W. Jantsch, and G. Weimann, Semicond. Sci. Technol. **5**, 686 (1990).

[12]H. Brugger, H. Müssig, C. Wölk, K. Kern, and D. Heitmann, Appl. Phys. Lett. **59**, 2739 (1991).

[13]P. B. Kriby, J. A. Constable, and R. S. Smith, Phys. Rev. B **40**, 3013 (1989).

[14]J. J. Harris, M. Brugmans, D. Dawson, J. P. Gowers, C. M. Hellon, J. Hewett, P. F. Fewster, C. Roberts, K. Woodbridge, and S. Auzoux, Semicond. Sci. Technol. **5**, 669 (1990).

[15]M. S. Skolnick, J. M. Rorison, K. J. Nash, D. J. Mowbray, P. R. Tapster, S. J. Bass, and A. D. Pitt, Phys. Rev. Lett. **58**, 2130 (1987).

[16]A. Dodabalapur, K. Sadra, and B. G. Streetman, J. Appl. Phys. **68**, 4119 (1990).

[17]S. K. Lyo and E. D. Jones, Phys. Rev. B **38**, 4113 (1988).

[18]L. V. Butov, V. D. Kulakovskii, T. G. Anderson, and Z. G. Chen, Phys. Rev. B **42**, 9472 (1990).

[19]Z. Wilamowski, W. Jantsch, G. Ostermayer, and J. Kossut, Mater. Sci. Forum **83-87**, 805 (1992).

[20]G. Livescu, D. A. B. Miller, D. S. Chemla, M. Ramaswamy, T. Y. Chang, N. Sauer, A. C. Gossard, and J. H. English, IEEE J. Quantum Electron. **24**, 1677 (1988).

[21]M. A. Herman, D. Bimberg, and J. Christen, J. Appl. Phys. **70**, R1 (1991).

[22]C. Herman and C. Weisbuch, Phys. Rev. B **15**, 823 (1977).

[23]W.-P. Hong, A. Zrenner, O. H. Kim, F. DeRosa, J. Harbison, and L. T. Florez, Appl. Phys. Lett. **57**, 1117 (1990).

[24]E. O. Kane, in *Tunneling Phenomena in Solids,* edited by E. Burstein and S. Lundqvist (Plenum, New York, 1969).

[25]E. E. Mendez, in *Physics and Applications of Quantum Wells and Superlattices,* Vol. 170 of *NATO Advanced Study Institute, Series B: Physics,* edited by E. E. Mendez and K. von Klitzing (Plenum, New York, 1987).

[26]O. Gunnarsson and B. I. Lundqvist, Phys. Rev. B **13**, 4274 (1976).

[27]C. Weisbuch and B. Vinter, *Quantum Semiconductor Structures Fundamentals and Applications* (Academic, Boston, 1991), Chap. 2.

[28]V. A. Altschul, A. Fraenkel, and E. Finkman, J. Appl. Phys. **71**, 4382 (1992).

[29]W. E. Spicer, P. W. Chye, P. R. Skeath, C. Y. Su, and I. Lindau, J. Vac. Sci. Technol. **16**, 1422 (1979).

[30]W. R. Miller and G. E. Stillman, Appl. Phys. Lett. **57**, 2934 (1990).